

Electronic Supplementary Information (ESI) for Lab on a Chip

This journal is © The Royal Society of Chemistry 2016

Electronic Supplementary Information

Construction of single-cell arrays and assay of cell drug-resistance in an integrated microfluidics

Long Pang,^a Wenming Liu,^b Chang Tian,^a Juan Xu,^b Tianbao Li,^b Shu-Wei Chen^b and Jinyi Wang^{a,b*}

^a*College of Veterinary Medicine, Northwest A&F University, Yangling, Shaanxi 712100, China.*

^b*College of Science, Northwest A&F University, Yangling, Shaanxi 712100, China.*

**Phone: + 86-29-870 825 20. Fax: + 86-29-870 825 20. E-mail: jywang@nwsuaf.edu.cn.*

Abstract. This Supplementary Information includes all additional information as noted in the text.

Supplementary Materials and Methods

Materials and reagents. RTV 615 poly(dimethylsiloxane) (PDMS) pre-polymer and curing agent were purchased from Momentive Performance Materials (Waterford, NY, USA). Surface-oxidized silicon wafers were from Shanghai Xiangjing Electronic Technology, Ltd. (Shanghai, China), AZ 50XT photoresist and developer from AZ Electronic Materials (Somerville, NJ, USA), and SU-8 2025 photoresist and developer from Microchem (Newton, MA, USA). Fluorescein diacetate (FDA), propidium iodide (PI) and bovine serum albumin (BSA) were obtained from Sigma-Aldrich (MO, USA). The DEVD-NucView 488 Caspase-3 assay kit and the JC-1 mitochondrial membrane potential detection kit were purchased from Biotium, Inc. (Hayward, CA). Cell culture medium, fetal bovine serum (FBS) and CellTracker Green CMFDA were from Gibco Invitrogen Corporation (CA, USA). Vincristine was purchased from Haizheng Pharmaceutical Co., Ltd (Zhejiang, China). The analytical reagent-grade solvents and other chemicals were purchased from local commercial suppliers, unless otherwise stated. All solutions were prepared using ultra-purified water supplied by a Milli-Q system (Millipore®).

Device fabrication. The microfluidic device utilized for this study was fabricated using the multilayer soft lithography method.^{S1} We designed the patterns of the device using the AutoCAD software. Generally, two different molds were first produced by photolithographic processes to create the fluidic components (channel width: 200 μm , height: 25 μm ; single cell separation and capture chamber width: 1500 μm , height: 25 μm , length: 3,600 μm , respectively.) and control channels (width: 100 to 200 μm ; height: 25 μm) embedded in the respective layers of the PDMS. To prepare the mold utilized for the fabrication of the fluidic components, a 25- μm thick positive photoresist (AZ 50XT, AZ Electronic

Materials) was spin-coated onto a silicon wafer. After UV exposure, the fluidic components on the wafer were developed using an AZ 400K developer (AZ Electronic Materials). To prepare the mold utilized for the fabrication of the control components, a 20- μm thick negative photoresist (SU8-2025, Micro. Chem) was spin-coated onto a silicon wafer. After UV exposure, the control components on the wafer were developed using the SU-8 developer (Micro. Chem). To achieve reliable performance of each valve, the widths of the control channels were set to 200 μm wide in the sections where the valve modules were located.

Before fabricating the microfluidic device, both the fluidic and control molds were exposed to trimethylchlorosilane (TMSCl) vapor for 2–3 min.^{S2} A well-mixed PDMS pre-polymer (RTV 615 A and B in 5 to 1 ratio) was then poured onto the fluidic mold placed in a Petri dish to yield a 3-mm thick fluidic layer. Another portion of PDMS pre-polymer (RTV 615 A and B in 20 to 1 ratio) was spin-coated onto the control mold (1600 rpm, 60 s, ramp 15 s) to obtain the thin control layer. The thick fluidic layer and the thin control layer were cured in an 80 °C oven for 50 min. After incubation, the thick fluidic layer was peeled off the mold, and holes were introduced into the fluidic layer for cell and reagent access, chamber purging, and waste exclusion. The fluidic layer was then trimmed, cleaned, and aligned onto the thin control layer. After baking at 80 °C for 60 min, the assembled layers were peeled off the control mold, and another set of holes was punched for access of control channels. These assembled layers were then placed on top of a glass slide coated (3000 rpm, 60 s, ramp 15 s) with PDMS pre-polymer (GE RTV 615 A and B in 10 to 1 ratio) that had been cured for 15 min in the oven (80 °C). The microfluidic device was ready for use after baking at 80 °C for 48 h.

Control interface. The control setup consisted of the eight-channel manifold (Ningbo Lida Pneumatic

Co., Ltd., Ningbo, China) controlled through a NI-PCI-6513 controller board (National Instruments, Austin, TX, USA) connected to a computer through a USB port. Nitrogen gas provided pressure (25 psi) to the manifolds. The control channels in the microfluidic device were first filled with water and were individually connected to the corresponding channels on the manifolds with metal pins (23 Gauge, Jinke Wei Corp, China) using polyethylene microbore tubing. When a regulator on the manifold was activated, nitrogen gas entered the respective control line connected with the regulator, providing pressure to closed valves in the microfluidic device. The control interface was created using Lab VIEW program (Version 8.0, National Instrument Inc.) on a personal computer, allowing for manual control of individual valves and automation of the microfluidic system.

Cell sample preparation. Two types of glioblastoma cells (normal U251 and induced U251 cells) were used to evaluate the capability of the device to separate and trap single cells with different size and deformability. Firstly, normal U251 and induced U251 cells were cultured separately. Afterward, to facilitate the observation during cell infusion and single cell capture, these tumor cells were stained with green fluorescence dye following the method reported previously.^{S4} Briefly, the normal and induced U251 cells were re-suspended separately in a pre-warmed Cell Tracker Green CMFDA solution to stain for 30 min in a humidified atmosphere with 5% CO₂ at 37 °C. Then, the tumor cells were resuspended in the cell buffer (PBS, 0.01 mol/L, PH 7.4; citric acid, 4.8 g/L; trisodium citrate, 13.2 g/L; and dextrose, 14.7 g/L) with 1% bovine serum albumin at a density of 100 000 cells/mL.^{S2} To evaluate the effect of cell densities on the single cell isolation efficiency, the tumor cell suspensions were respectively diluted to the density of 5 000, 10 000, 15 000, 20 000, 25 000 and 30 000 cells/mL using the previous method.^{S3}

Cell size measurement. Before and after the on-chip experiments, the size of two types of U251 cells was measured. For the off-chip experiment, the tumor cells were collected by centrifugation at 2 000 rpm for 10 min after washing twice with PBS and treating with trypsin for 10 min. The cell numbers were counted using a hemocytometer and then cell suspension (in PBS) was diluted to 1×10^4 cells/mL with PBS. The diameter of the tumor cells were then measured. For the on-chip experiment, the diameter of the captured tumor cells were directly measured after the capture in the filter matrices. The measurement of cell size was performed based on the optical cell images, which were analyzed using Image-Pro® Plus 6.0 (Media Cybernetics, Silver Spring, MD) and SPSS 12.0 (SPSS Inc.) softwares. The diameter of the tumor cells in the off-chip or on-chip experiment, was an average value obtained from 300 cells.

Chemotherapy and cell viability of the control tests. For the control experiments, the cells were cultured using the conventional cell culture plate. Briefly, after removing the growth medium and washing with PBS, 2.5 μ M vincristine was introduced into the cell samples for 120 min. For cell viability assay, after removing the growth medium or vincristine and washing with PBS, the FDA/PI staining solution (10 μ g/mL each in PBS) was introduced into the cell samples and stained for 10 min at room temperature. Then, PBS was introduced for 5 min as a final rinse.

Mitochondrial membrane potential and caspase-3 activity of the control tests. After removing the growth medium or vincristine, the JC-1 (5 μ M in DMEM) was introduced directly into the cell samples and incubated for 15 min at 20 °C before PBS rinsing. The analysis of caspase-3 activation of the cells was performed by directly introducing NucView 488 caspase-3 substrate (1 μ M in DMEM) into the cell samples and incubating for 30 min at 20 °C before PBS rinsing.^{S4}

Numerical simulations. To evaluate the velocity field fluctuations in the device, computational fluid dynamics (CFD) simulation was performed using ESI-CFD software (V2010.0, ESI CFD, Inc.). The simulation environment was verified for steady incompressible flows. Constant flow rates were specified at the input, and the outlet was set to a fixed-pressure boundary condition. No slip boundary condition was applied at the channel walls. FLOW module in CFD-ACE+ were used to explore the flow velocity distribution in the microchannels. Based on the finite volume method, the conservation of Navier–Stokes momentum in the device is described by the equation (Eq. S1) as follows.^{S2}

$$\frac{\partial}{\partial t}(\rho \mathbf{V}) + \nabla \cdot (\rho \mathbf{V} \mathbf{V}) = -\nabla P + \nabla \cdot \bar{\tau} \quad (\text{Eq. S1})$$

The conservation of mass is described by the continuity equation (Eq. S2) as follows.

$$\frac{\partial \rho}{\partial t} + \nabla \cdot (\rho \mathbf{V}) = 0 \quad (\text{Eq. S2})$$

where ρ is the fluid density, $\rho \mathbf{V}$ is the velocity vector of the fluid, P is the pressure and $\bar{\tau}$ is the stress tensor.

Single cell isolation and collection efficiency. For the study of single cell isolation and distribution, single cell isolation efficiency calculated using the following equation (Eq. S3).

$$\text{Single cell isolation efficiency} = \frac{\text{Single cell}_{\text{filter matrices}}}{\text{Tumor Cell}_{\text{filter matrices}}} \times 100\% \quad (\text{Eq. S3})$$

Where $\text{Single cell}_{\text{filter matrices}}$ is the single cells captured in the filter matrices, $\text{Tumor Cell}_{\text{filter matrices}}$ is all the cells captured in the filter matrices.

The collection efficiency of cells was calculated using the following equation (Eq. S4).

$$\text{Collection efficiency} = \frac{\text{Tumor Cell}_{\text{filter matrices}}}{\text{Tumor Cell}_{\text{inlet}}} \times 100\% \quad (\text{Eq. S4})$$

Where $\text{Tumor Cell}_{\text{filter matrices}}$ is the cells captured in the filter matrices, $\text{Tumor Cell}_{\text{inlet}}$ is the cells infused into the device from the cell inlet.

The cell distribution rate in each filter matrix was calculated using the following equation (Eq. S5).

$$\text{Cell distribution rate} = \frac{\text{Tumor Cell}_{\text{filter matrix}}}{\text{Tumor Cell}_{\text{filter matrices}}} \times 100\% \quad (\text{Eq. S5})$$

Where $\text{Tumor Cell}_{\text{filter matrix}}$ is the cells captured in each filter matrix, $\text{Tumor Cell}_{\text{filter matrices}}$ is the cells captured in all the filter matrices.

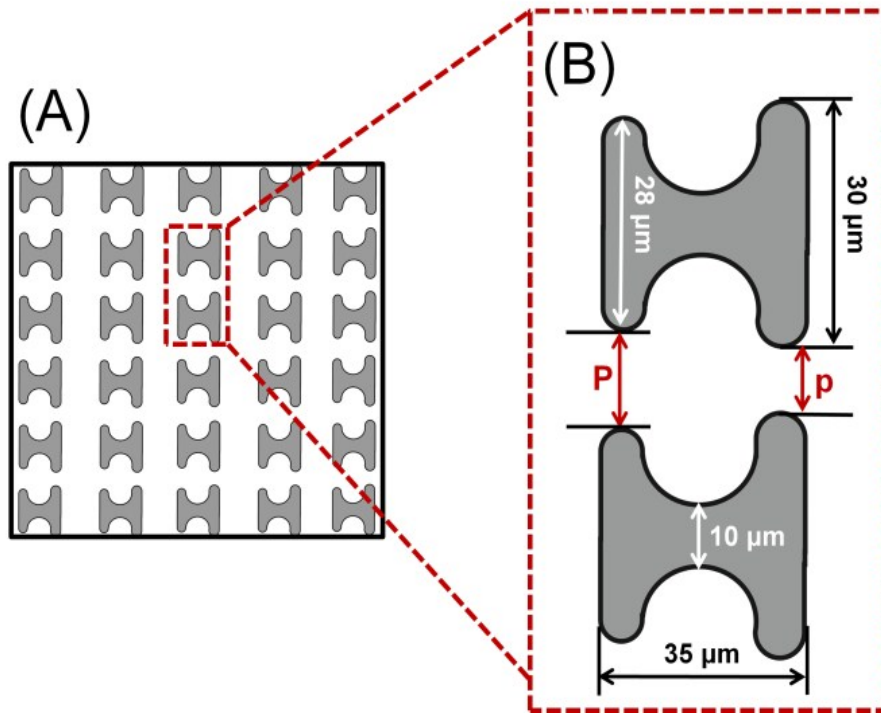


Figure S1. (A) Schematic diagram of one filter matrix. Each filter matrix in the device is composed of 5 columns and many rows (from input to output of the device the rows are 36, 38, 39, 40, and 41, respectively). (B) One filter unit composed of two neighbouring H-shaped microstructures. For each filter unit, the first pore size (P) is 2 μm larger than the second pore size (p).

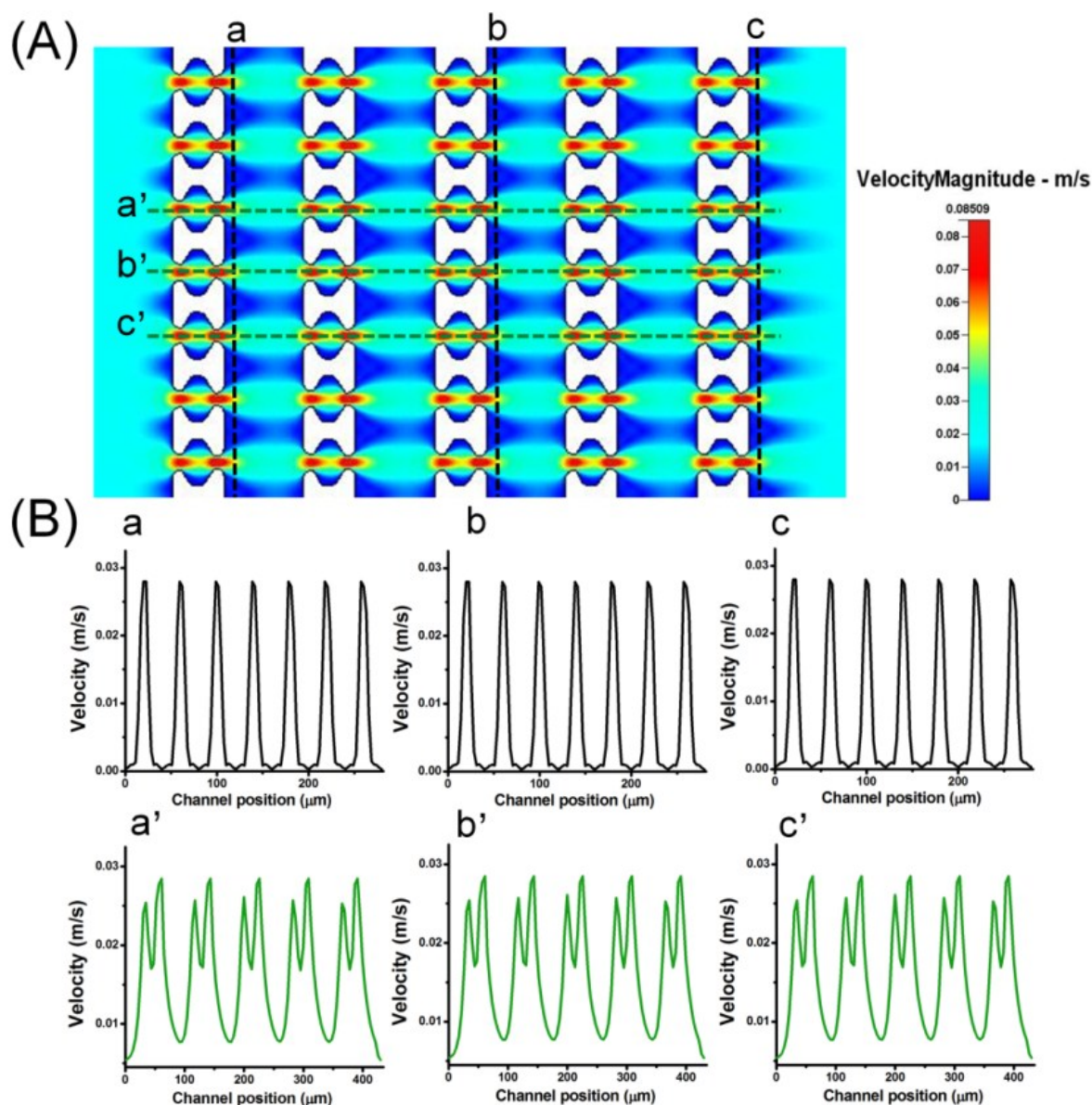


Figure S2. Computational simulation of the fluid velocities in the 10- μm filter matrix (i.e., the second pore size of the filter matrix is 10 μm) at the flow rate of 50 $\mu\text{L}/\text{min}$ (the velocity magnitude is 0.018 m/s). (A) Fluid velocity pattern formed in the 10- μm filter matrix. The dotted lines (a, b, c, a', b' and c') were used to analyze the fluid velocity distributions in the 10- μm filter matrix. (B) Quantitative analysis of the fluid velocities in the 10- μm filter matrix at the velocity magnitude of 0.018 m/s, which correspond to the positions of the dotted lines (a, b, c, a', b' and c') in (A), respectively.

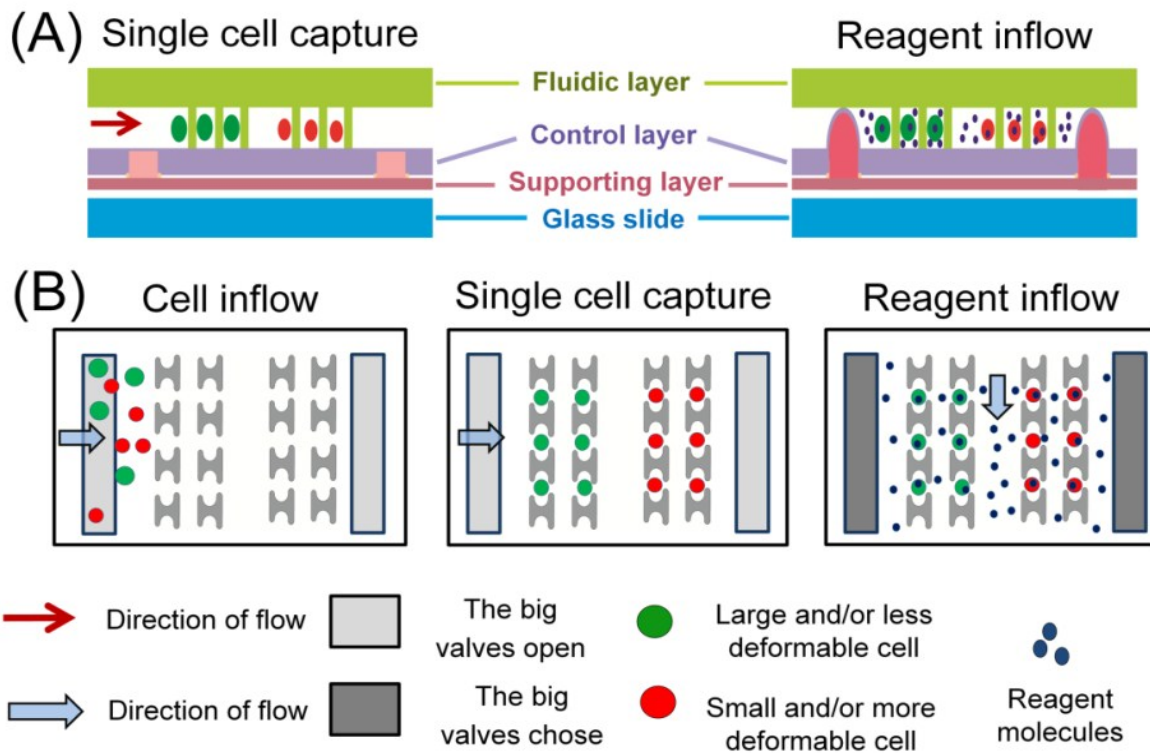


Figure S3. (A) Schematic diagram of the lateral view of single cells sorting and reagent infusion in the microfluidic device, which also showed that the device consisted of four layers: fluidic layer, control layer, supporting layer and glass slide. (B) Schematic diagrams showing the operation of the microvalves during cell infusion, single cell capture and reagent infusion. During the cell infusion and single cell capture steps, the vertical microvalves were opened to allow the cell sample to flow through the filter matrices for single cells sorting according to their size and deformability. During the reagent infusion, the big microvalves were closed to allow the reagent infusion through the filter matrix.

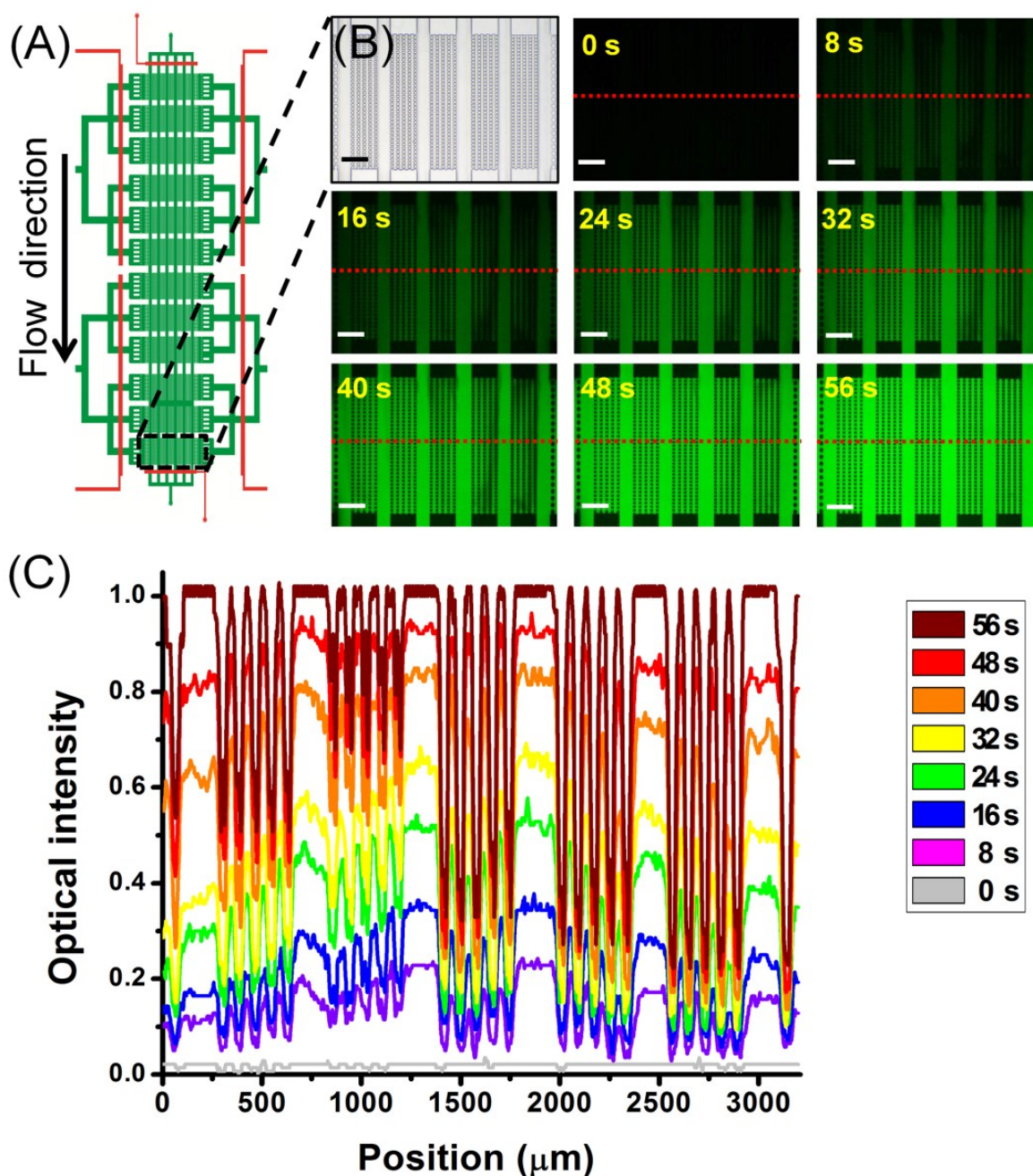


Figure S4. Analysis of the mass transportation and distribution in the device. The flow rate is 15 $\mu\text{L}/\text{min}$.

(A) Schematic diagram of the designed microdevice. Green indicates the fluidic channels and red indicates the valves. (B) Observable mass distribution in the device at different times. During this study, the reagent inlet and waste outlet 2 were opened, and the cell inlet and waste outlet 1 were closed by operating the microvalve system. Scale bar is 300 μm . (C) Quantitative concentration distribution at different times, corresponding to the dotted lines in (B).

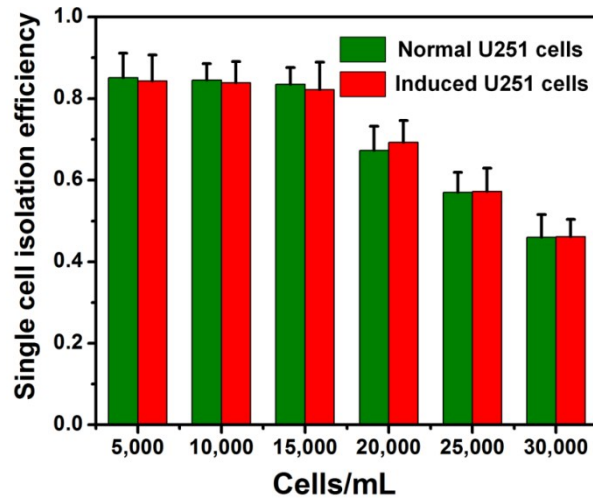


Figure S5. The isolation efficiency of the single cells in the device under different cell densities, indicating that the single cell isolation efficiency at low cell densities (5 000, 10 000, and 15 000 cells/mL) are higher than those at the high cell densities (20 000, 25 000, 30 000 cells/mL). The infusion flow rate is 80 μ L/min. Standard deviations deduced from ten parallel experiments were shown as the error bars.

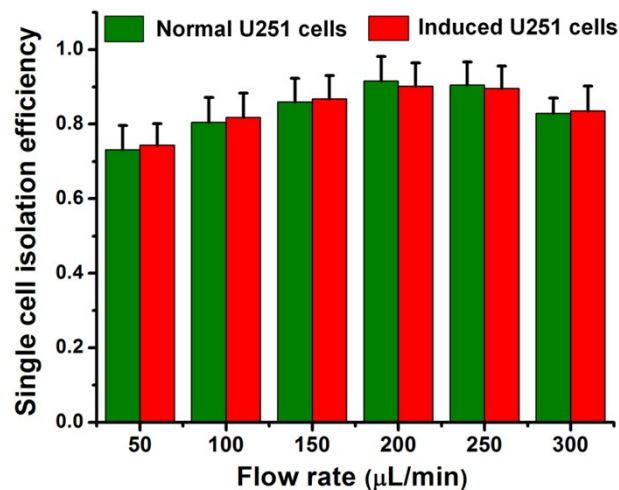


Figure S6. The isolation efficiency of single cells in the device under different infusion flow rates. The cell density is 15 000 cells/mL. Standard deviations deduced from ten parallel experiments were shown as the error bars.

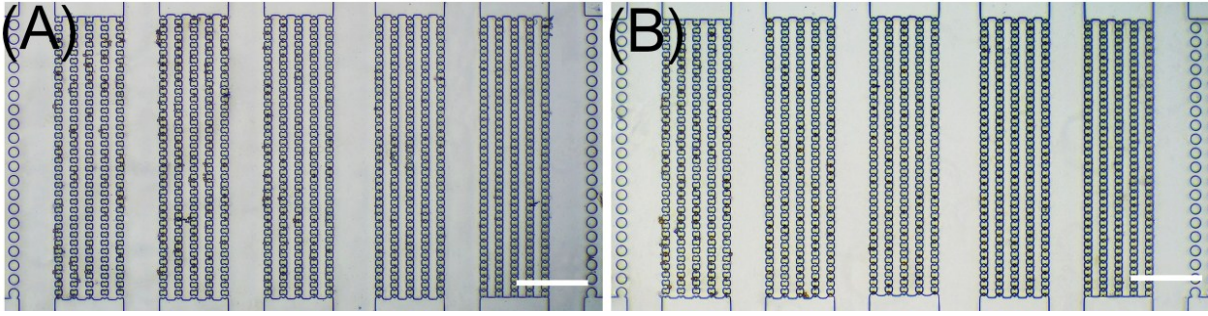


Figure S7. Generation of single-cell arrays in the filter matrices under the optimum conditions: infusion cell density is 15 000 cells/mL and the infusion flow rate is 200 $\mu\text{L}/\text{min}$. (A) Bright-field image of the normal U251 cells captured in the filter matrices. Fluorescence image of the normal U251 cells captured in the filter matrices was shown in Figure 2A. (B) Bright-field image of the induced U251 cells captured in the filter matrices. Fluorescence image of the induced U251 cells captured in the filter matrices was shown in Figure 2B. Scale bars in (A) and (B) are 400 μm .

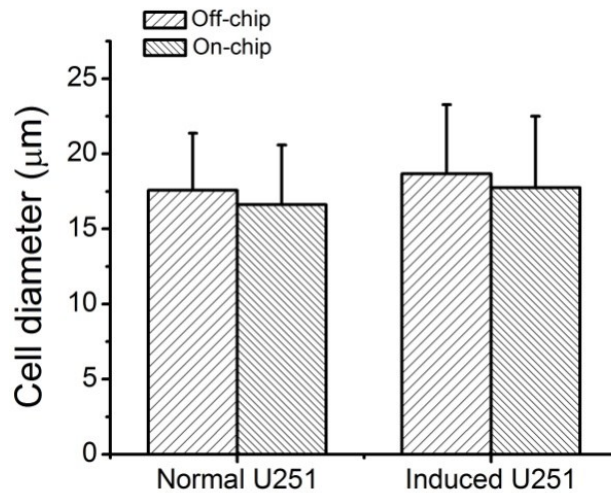


Figure S8. Quantitative on- and off-chip analysis of the cell size. The results indicated that the diameter of cells captured in the device was similar to that of the conventional cultured cells in the culture plates.

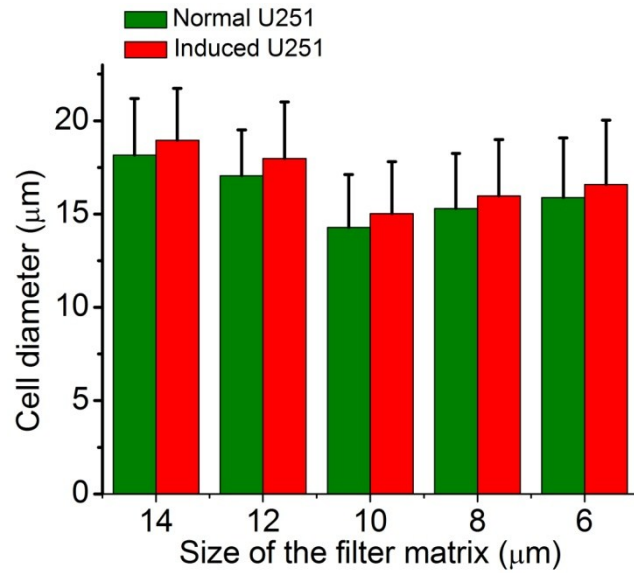


Figure S9. The cell diameter of normal U251 cells and induced U251 cells in different filter matrices.

The diameter of the tumor cells was an average value obtained from images of 300 cells.

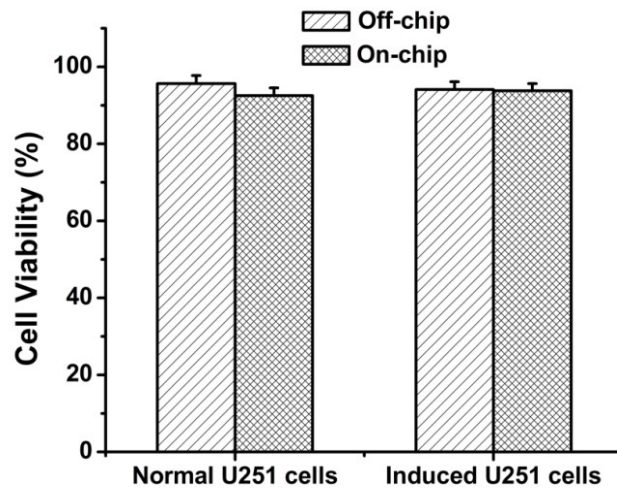


Figure S10. Quantitative analysis of the on- and off-chip cell viability by using FDA/PI double-staining protocol, indicating that the single cells captured in the device remain highly viable, similar to off-chip cultured cells, retrieving >92% viable cells. Standard deviations deduced from ten parallel experiments were shown as the error bars.

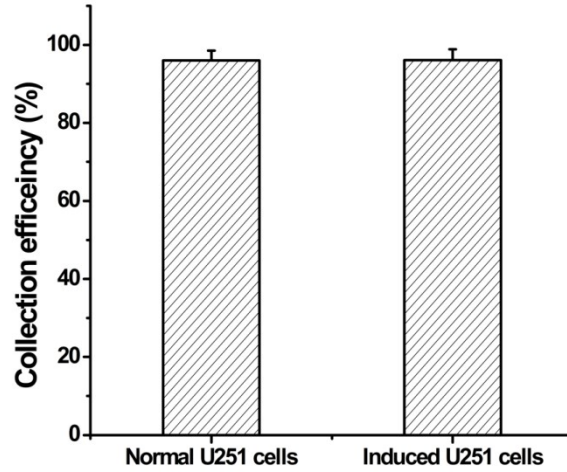


Figure S11. Statistical collection efficiency of the single normal and induced U251 cells in the device. Each type of cells was independently tested using the optimized parameters. Standard deviations deduced from ten parallel experiments were shown as the error bars.

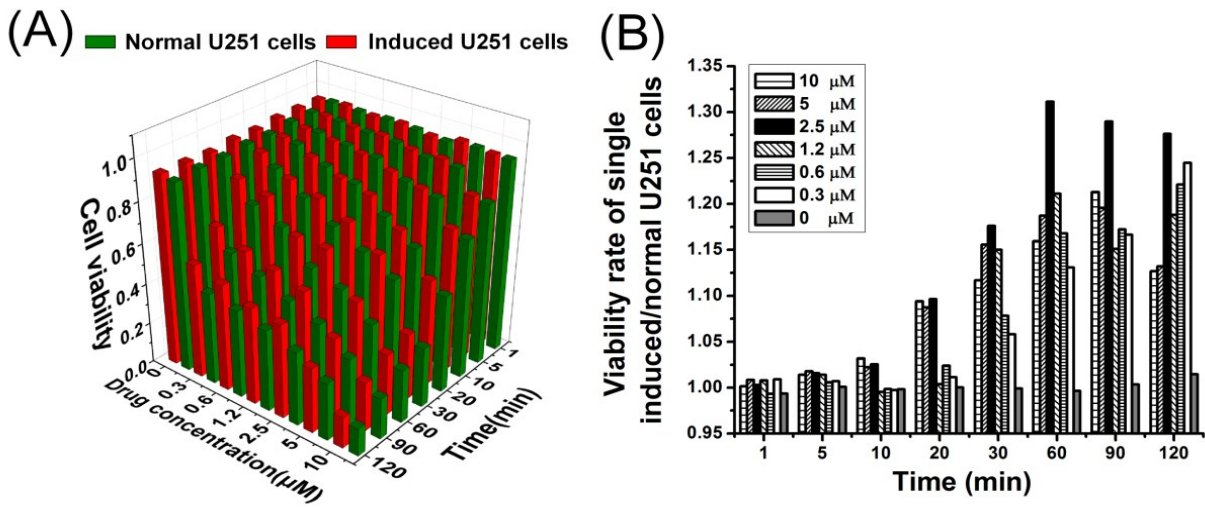


Figure S12. (A) The statistical cell viability after different time and vincristine concentration treatments. (B) The ratios of the single induced/normal U251 cell viabilities were used to reflect the quantitative dynamics of the cell viability during chemotherapy, corresponding to (A).

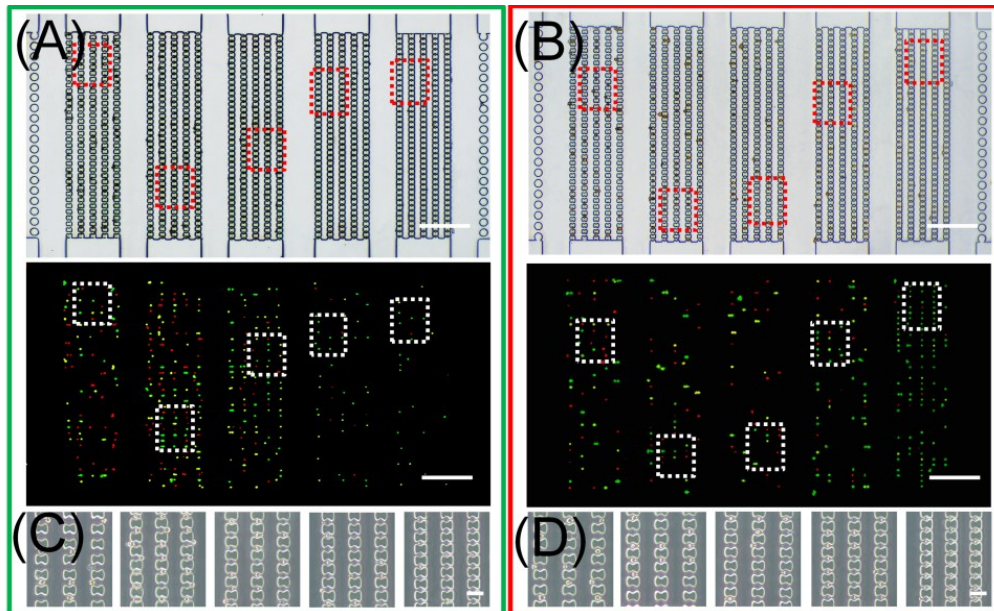


Figure S13. The viability assay of the single cells captured in different filter matrices after 60-min treatment with 2.5 μM vincristine. (A and B) Bright-field and fluorescence images of the normal (A) and induced (B) U251 cells. Scale bars in (A) and (B) are 400 μm . (C and D) Magnified bright-field images of (A) and (B), respectively. Fluorescence images of the normal U251 cells (C) and the induced U251 cells (D) after vincristine treatment were shown in Figure 3A. Scale bars in (C) and (D) are 40 μm .

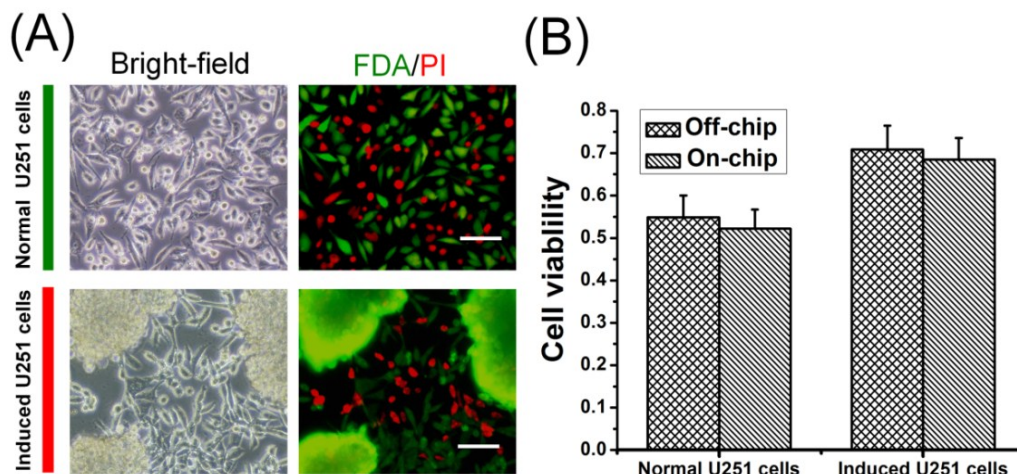


Figure S14. Comparison of the on- and off-chip cell viabilities after 60-min treatment with 2.5 μM vincristine. (A) The bright-field (left) and fluorescence (right) images of the off-chip (control) normal (the first row) and induced (the second row) U251 cells. (B) Quantitative analysis of cell viabilities of the on-

and off-chip U251 cells. The results confirmed that the on-chip cell viability is similar to the off-chip (control) cells. Scale bars, 100 μm . Standard deviations deduced from ten parallel experiments were shown as the error bars.

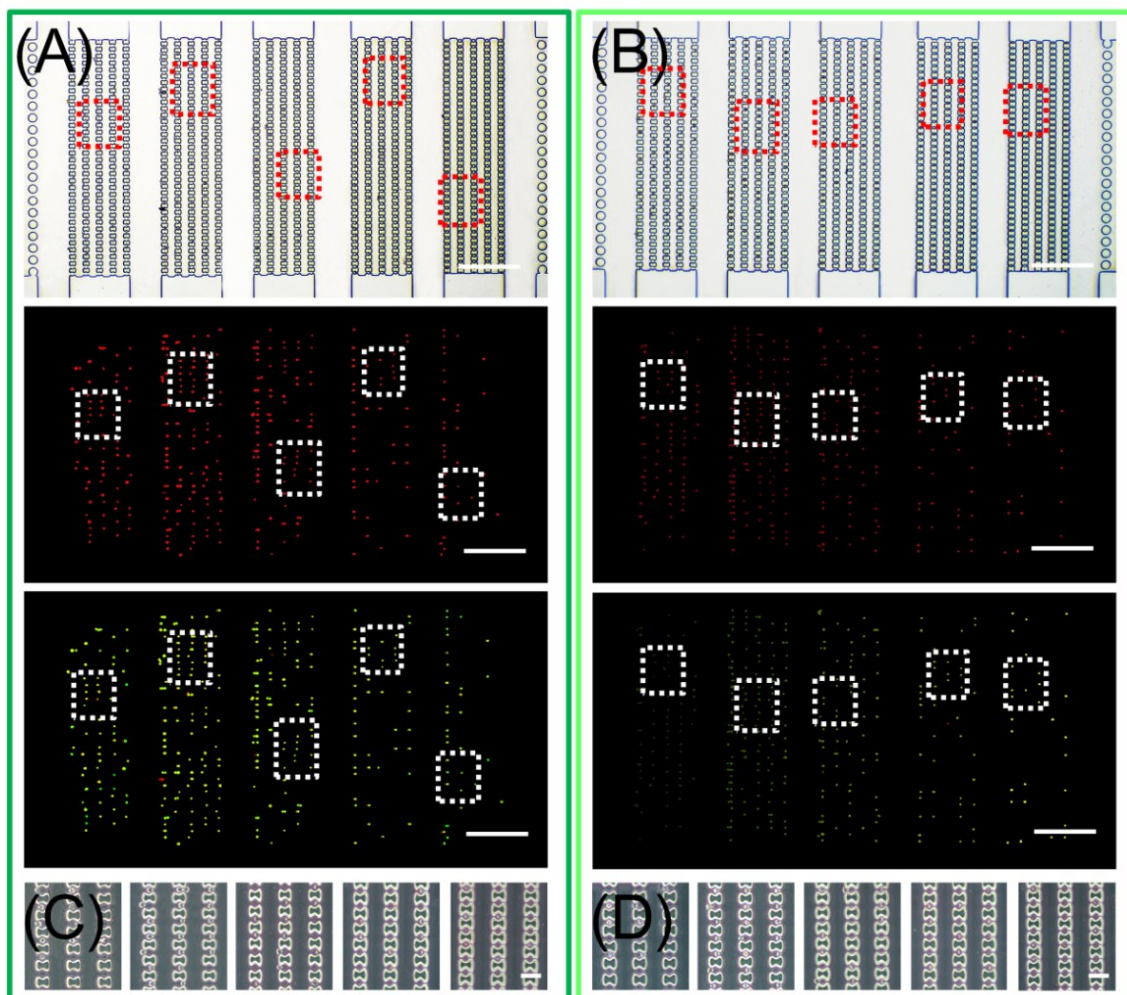


Figure S15. Mitochondrial membrane potential of the single normal U251 cells captured in different filter matrices of the device. (A) Bright-field and JC-1 aggregate (red) and monomer (green) fluorescence images of the normal U251 cells before vincristine treatment. (B) Bright-field and JC-1 aggregate (red) and monomer (green) fluorescence images of the normal U251 cells after 60-min treatment with vincristine. Scale bars in (A) and (B) are 400 μm . (C and D) Magnified bright-field of (A) and (B), respectively. Fluorescence image of the normal U251 cells before vincristine treatment (C) was shown in

Figure S20, and the normal U251 cells after 60-min vincristine treatment (D) was shown in Figure 3C.

Scale bars in (C) and (D) are 40 μm .

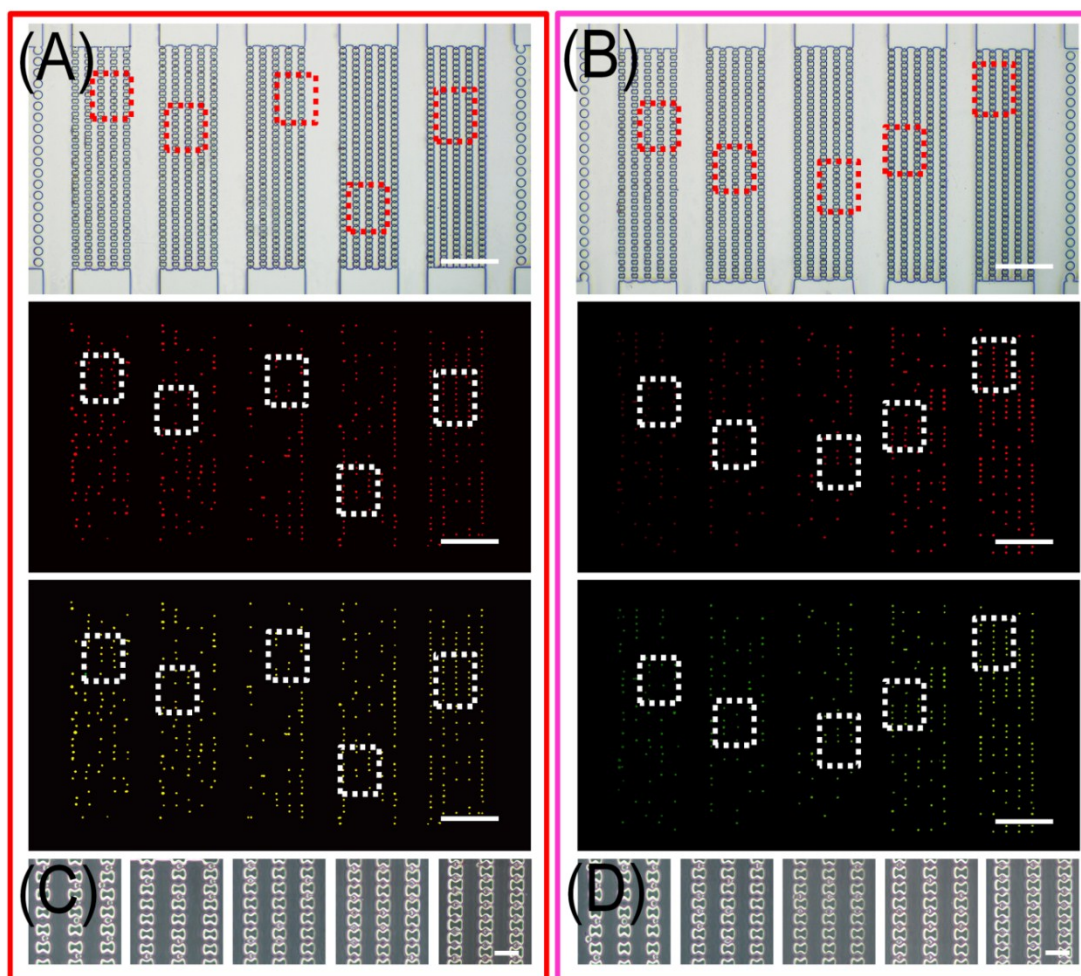


Figure S16. Mitochondrial membrane potential of the single induced U251 cells captured in different filter matrices of the device. (A) Bright-field and JC-1 aggregate (red) and monomer (green) fluorescence images of the induced U251 cells before vincristine treatment. (B) Bright-field and JC-1 aggregate (red) and monomer (green) fluorescence images of the induced U251 cells after 60-min vincristine treatment. Scale bars in (A) and (B) are 400 μm . (C and D) Magnified bright-field of (A) and (B), respectively. Fluorescence image of the induced U251 cells before vincristine treatment (C) was shown in Figure S21, and the induced U251 cells after 60-min vincristine treatment (D) was shown in Figure S21. Scale bars in

(C) and (D) are 40 μm .

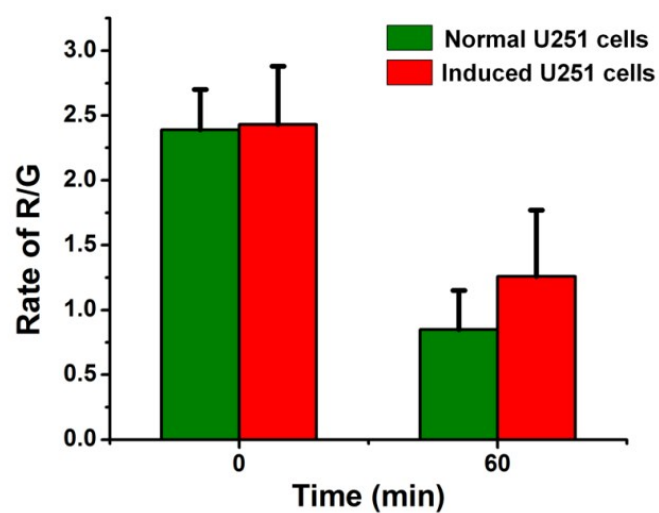


Figure S17. Ratios of JC-1 aggregate (red) to its monomer (green) in the normal and induced U251 cells before and after 2.5 μM vincristine treatment. Standard deviations deduced from ten parallel experiments were shown as the error bars.

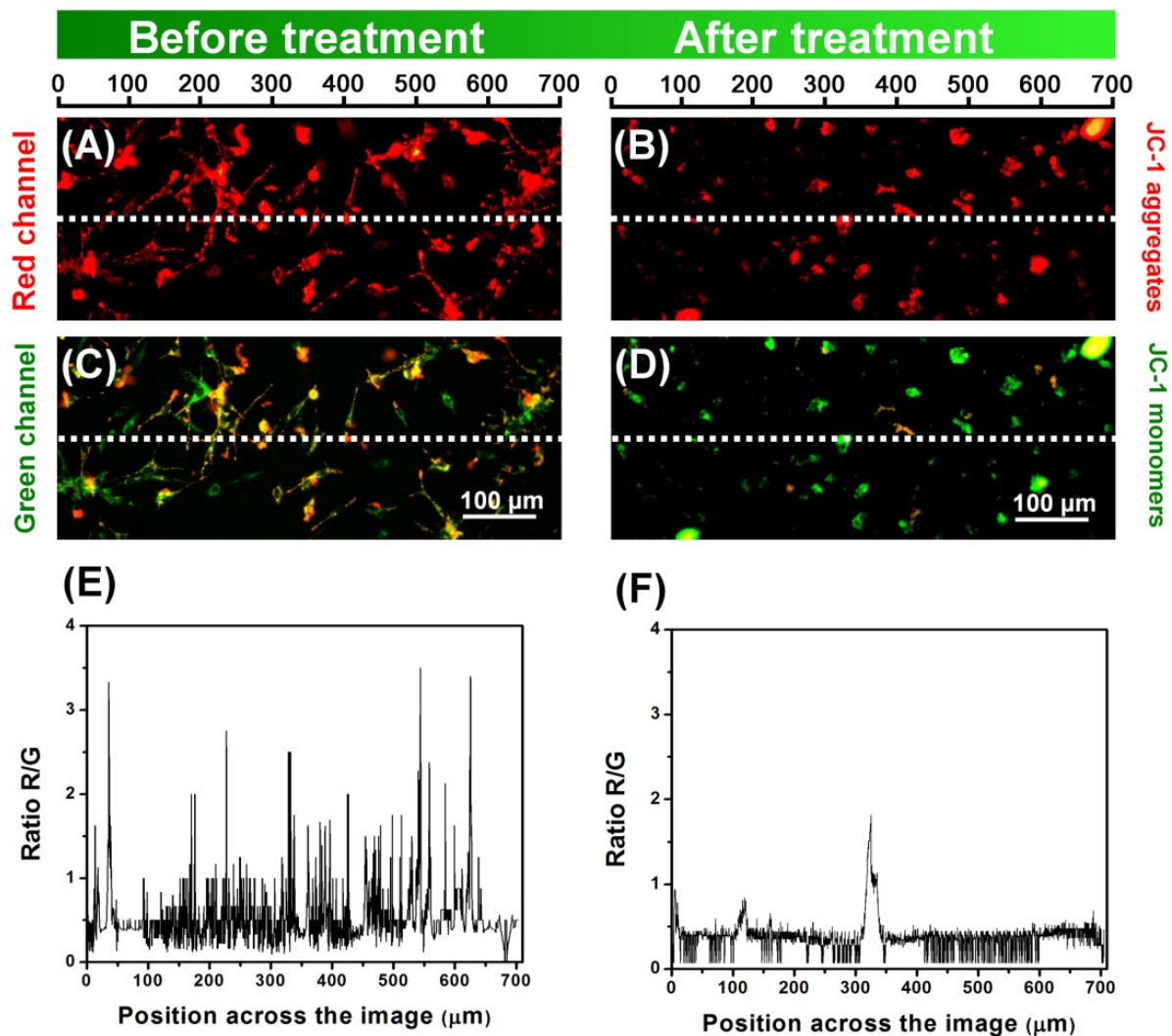


Figure S18. Mitochondrial membrane potential of the normal U251 cells cultured using the conventional plate-based method. (A and B) Fluorescence images of JC-1 aggregates in the mitochondria of normal U251 cells before (A) and after (B) 60-min treatment with 2.5 μM vincristine. (C and D) Fluorescence images of JC-1 monomers in the cytoplasm of normal U251 cells before (C) and after (D) 60-min treatment with 2.5 μM vincristine. (E and F) Ratios of JC-1 aggregate to its monomer before (E) and after (F) 60-min treatment with 2.5 μM vincristine, corresponding to the dotted lines in (A) and (C), as well as (B) and (D), respectively.

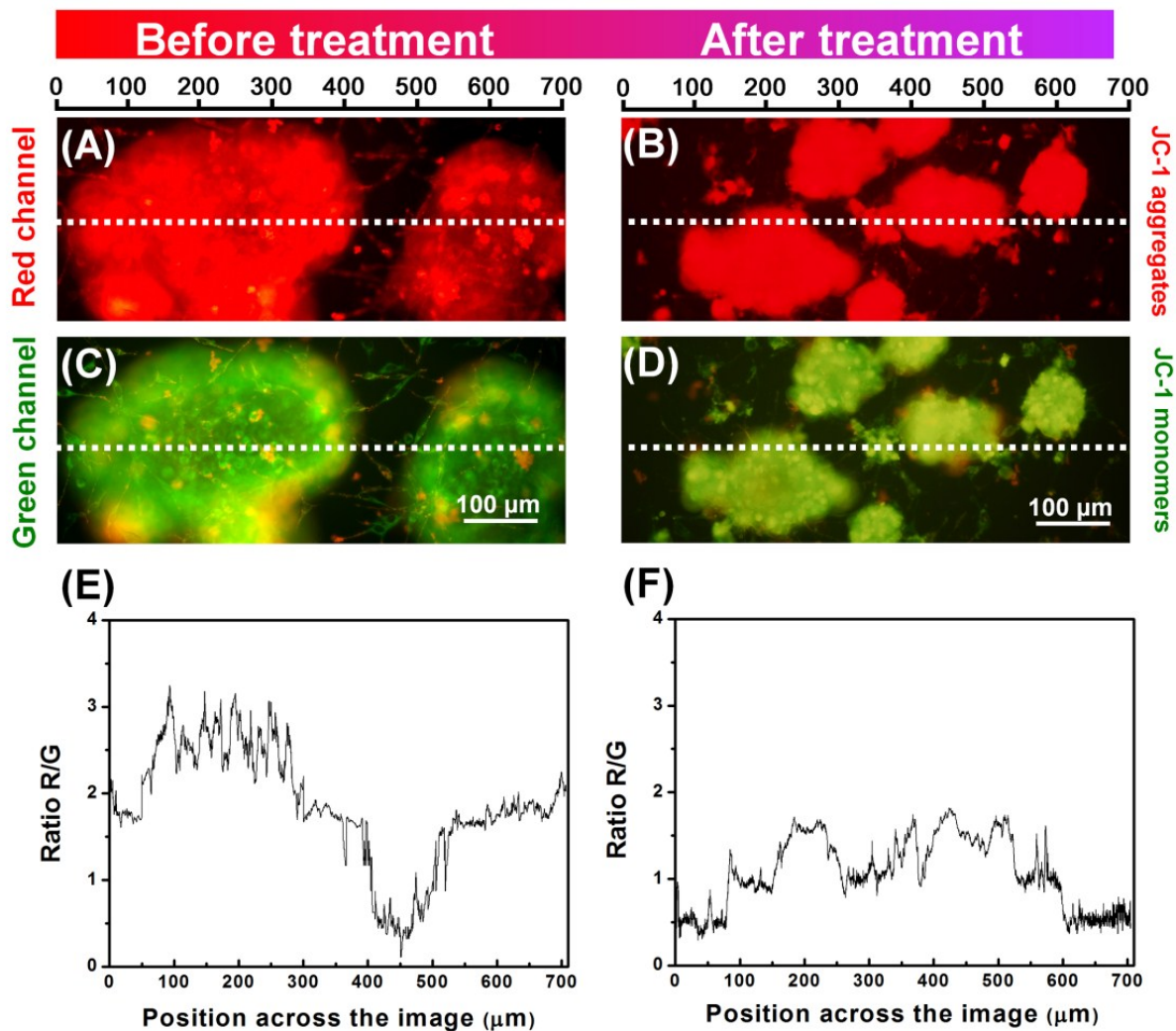


Figure S19. Mitochondrial membrane potential of the induced U251 cells cultured using the conventional plate-based method. (A and B) Fluorescence images of JC-1 aggregates in the mitochondria of induced U251 cells before (A) and after (B) 60-min treatment with 2.5 μM vincristine. (C and D) Fluorescence images of JC-1 monomers in the cytoplasm of induced U251 cells before (C) and after (D) 60-min treatment with 2.5 μM vincristine. (E and F) Ratios of JC-1 aggregate to its monomer before (E) and after (F) 60-min treatment with 2.5 μM vincristine, corresponding to the dotted lines in (A) and (C), as well as (B) and (D), respectively.

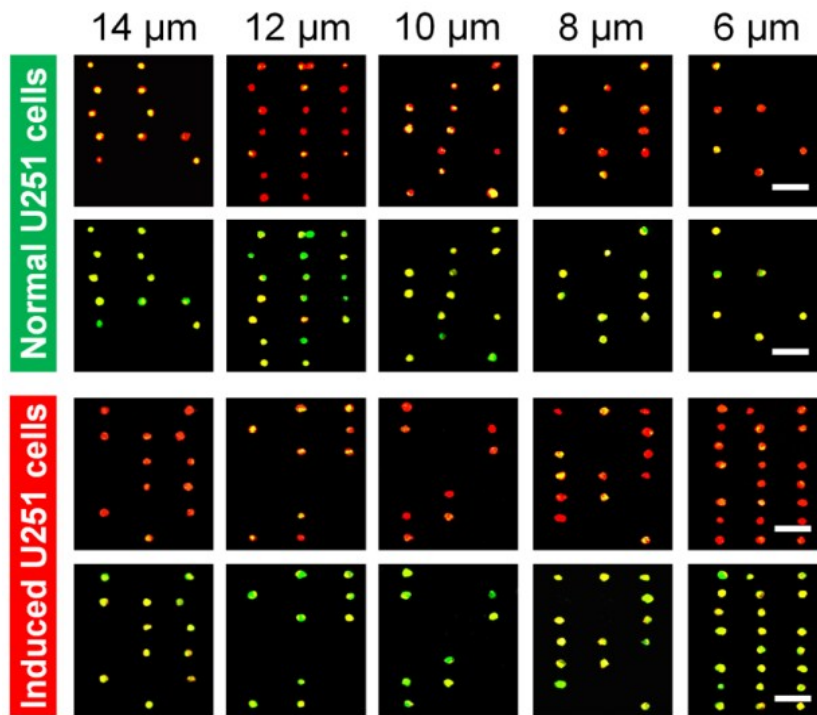


Figure S20. Mitochondrial membrane potential of the single cells captured in different filter matrices of the device. JC-1 aggregate (red) and monomer (green) fluorescence images of the normal U251 cells (rows 1 and 2) and induced U251 cells (rows 3 and 4) before vincristine treatment. Scale bars are 60 μm. The sizes of the filter matrices are the sizes of the second pores in each filter matrix.

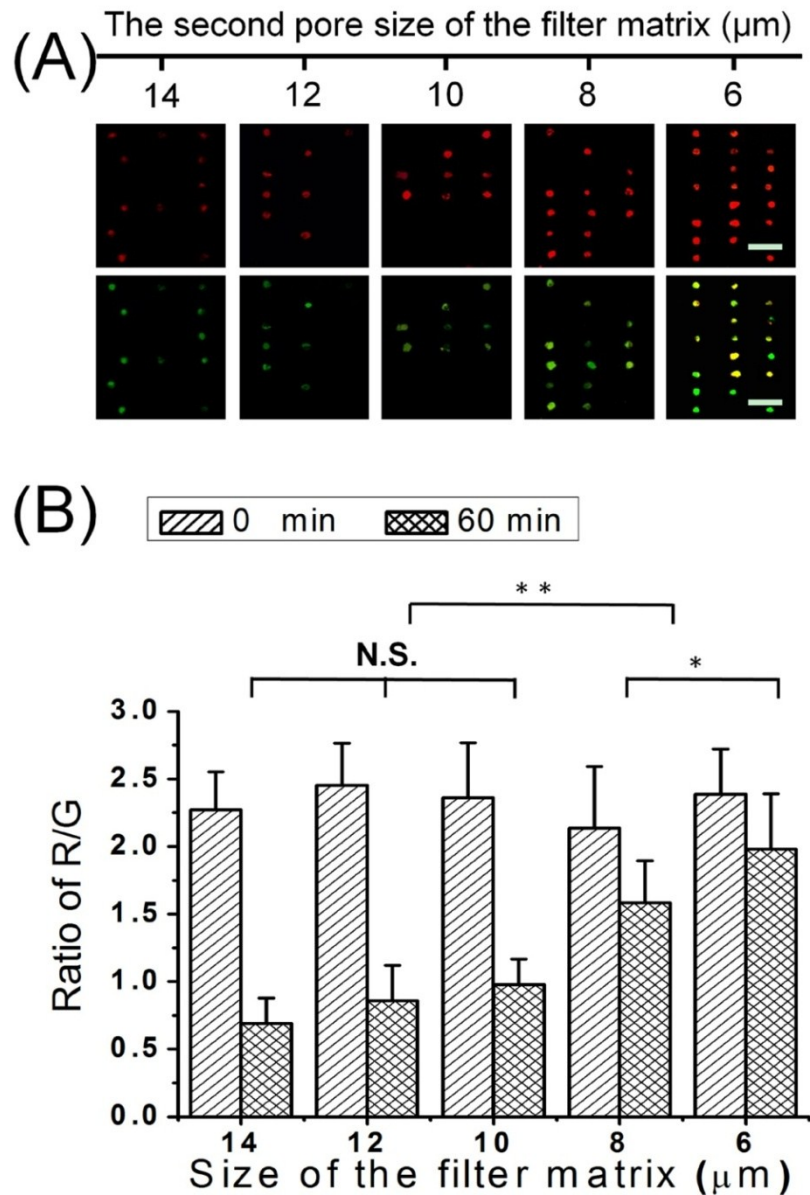


Figure S21. Mitochondrial membrane potential of the single induced U251 cells captured in different filter matrices of the device after 60-min treatment with 2.5 μM vincristine. (A) JC-1 aggregate (red) and monomer (green) fluorescence images of the induced U251 cells after vincristine treatment. Scale bars are 60 μm . (B) The statistical ratios of JC-1 aggregate to its monomer in the induced U251 cells after vincristine treatment. The sizes of the filter matrices are the sizes of the second pores in each filter matrix. Standard deviations deduced from ten parallel experiments are shown as the error bars, with the significance assessed by ANOVA. ** $P < 0.01$; * $P < 0.05$; N.S., not significant.

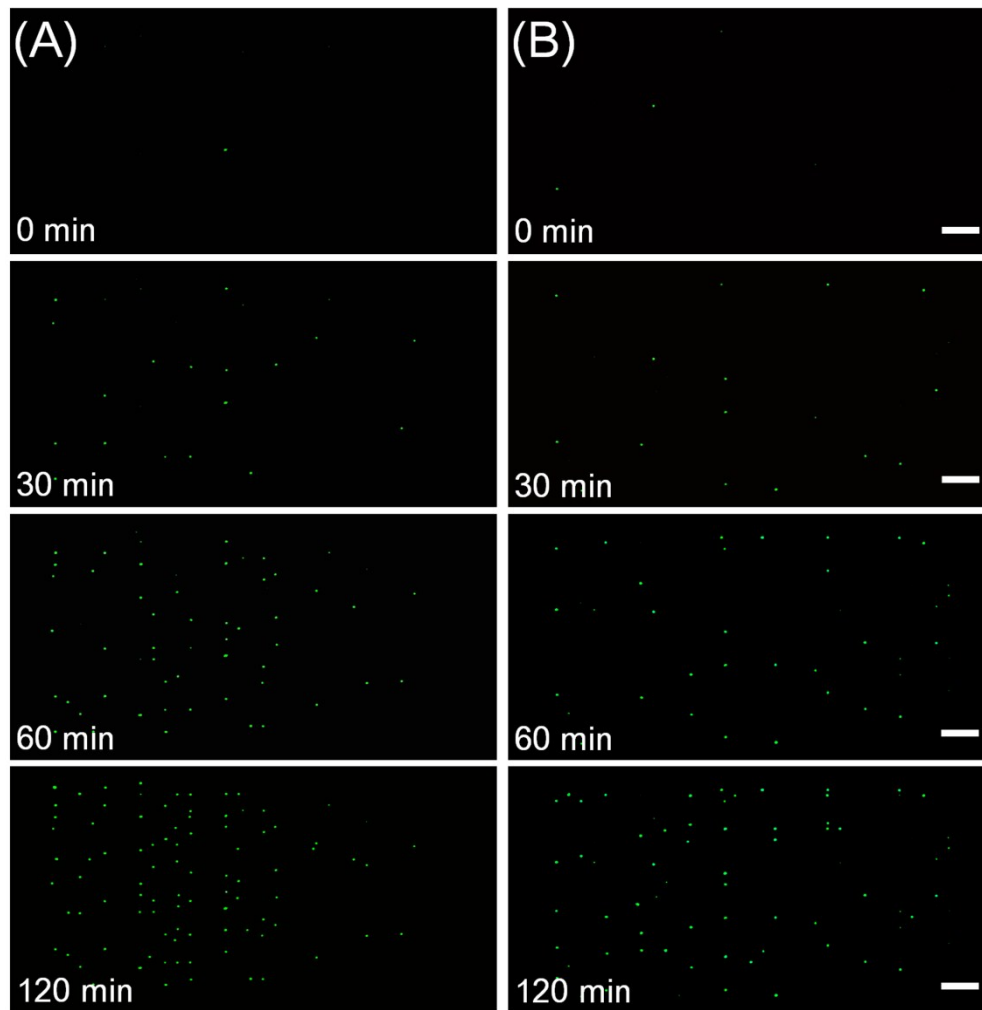


Figure S22. Caspase-3⁺ cells captured in the filter matrices of the device after different time treatments with 2.5 μM vincristine. (A) Temporal fluorescence images of the caspase-3⁺ normal U251 cells. (B) Temporal fluorescence images of the caspase-3⁺ induced U251 cells. Scale bars in (A) and (B) are 250 μm .

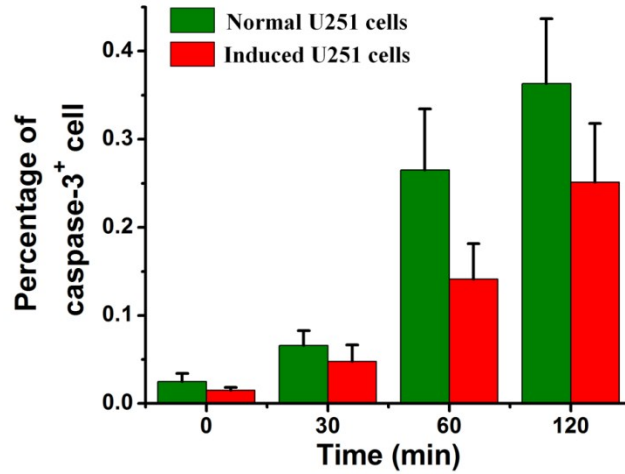


Figure S23. On-chip caspase-3 activation (caspase-3⁺) of the normal and induced U251 cells after different time treatments with 2.5 μM vincristine. Standard deviations deduced from ten parallel experiments were shown as the error bars.

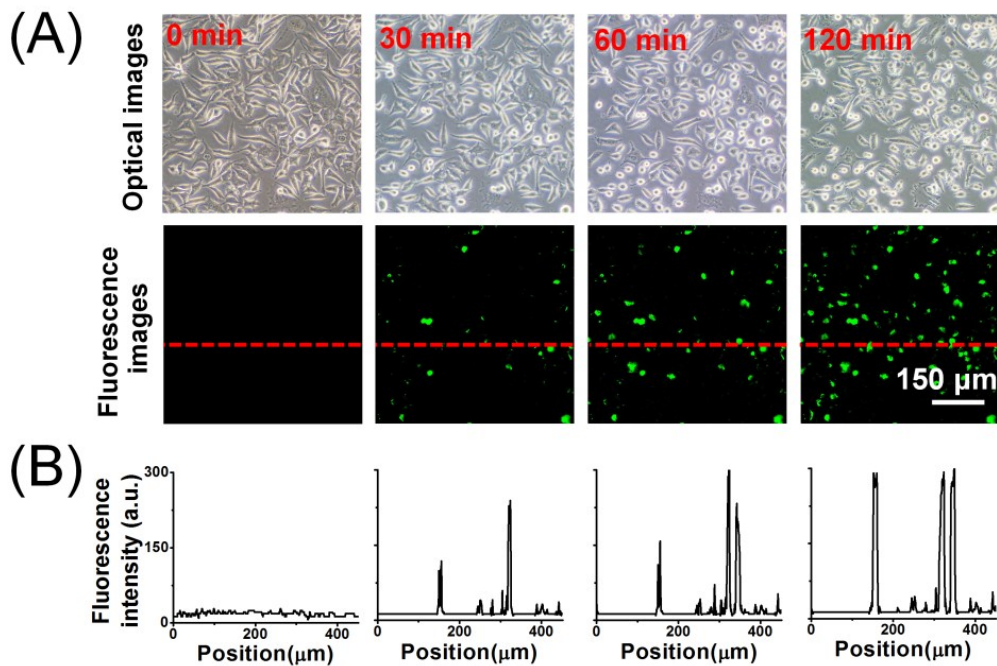


Figure S24. Off-chip caspase-3 activation of the normal U251 cells after different time treatments with 2.5 μM vincristine. (A) Fluorescent images of caspase-3⁺ normal U251 cells after different time treatments with 2.5 μM vincristine. (B) Fluorescence intensity distribution of the caspase-3⁺ cells at various treatment times (from left to right: 0, 30, 60, 120 min, respectively), corresponding to the dotted line in (A).

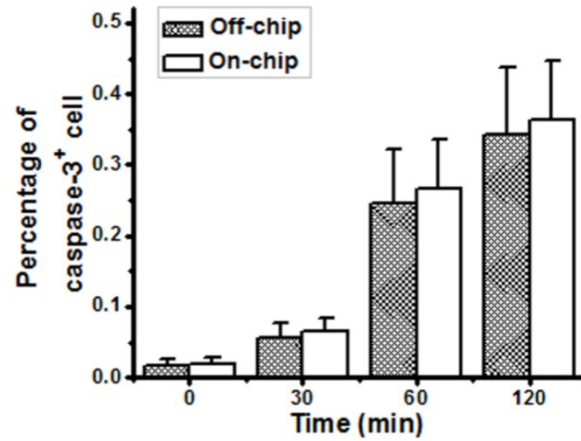


Figure S25. Quantitative percentages of the caspase-3⁺ normal U251 cells after on- and off-chip vincristine treatments. Standard deviations deduced from ten parallel experiments were shown as the error bars.

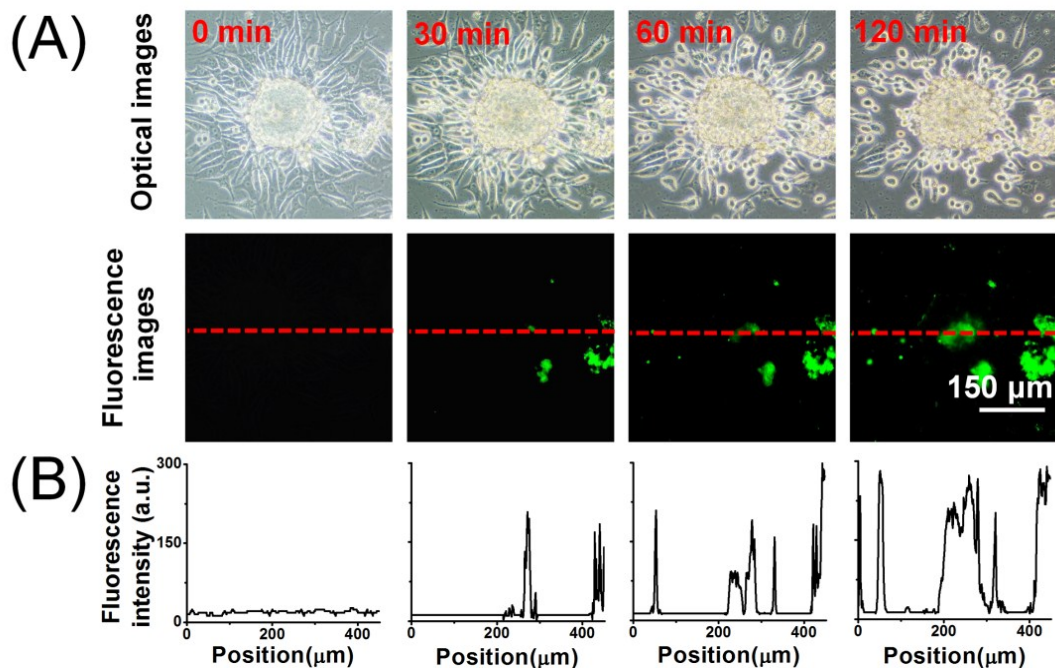


Figure S26. Off-chip caspase-3⁺ cells of the induced U251 cells after different time treatments with 2.5 μM vincristine. (A) Fluorescent images of caspase-3⁺ induced U251 cells after different time treatments with 2.5 μM vincristine. (B) Fluorescence intensity distribution of the caspase-3⁺ cells at various treatment times (from left to right: 0, 30, 60, 120 min, respectively), corresponding to the dotted line in (A).

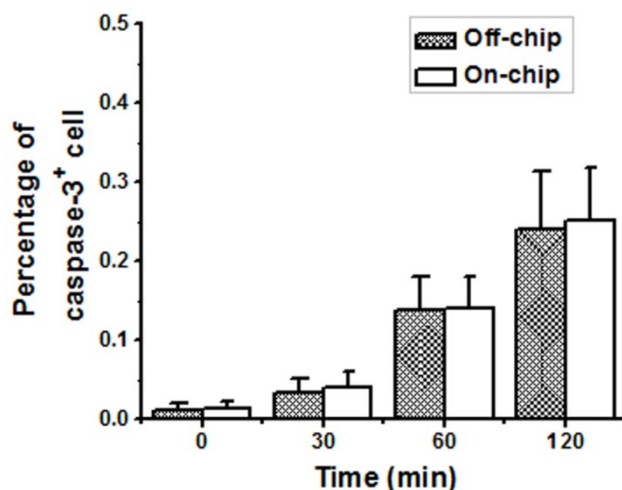


Figure S27. Quantitative percentages of the caspase-3⁺ induced U251 cells after on- and off-chip vincristine treatments. Standard deviations deduced from ten parallel experiments were shown as the error bars.

References for the ESI.

- (S1) Y. J. Wang, W. Y. Lin, K. Liu, R. J. Lin, M. Selke, H. C. Kolb, N. G. Zhang, X. Z. Zhao, M. E. Phelps, C. K. F. Shen, K. F. Faull and H. R. Tseng, *Lab Chip*, 2009, **9**, 2281-2285.
- (S2) S. F. Shen, C. Ma, L. Zhao, Y. L. Wang, J. C. Wang, J. Xu, T. B. Li, L. Pang and J. Wang, *Lab Chip*, 2014, **14**, 2525-2538.
- (S3) L. Pang, S. F. Shen, C. Ma, T. T. Ma, R. Zhang, C. Tian, L. Zhao, W. M. Liu and J. Wang, *Analyst*, 2015, **140**, 7335-7346.
- (S4) L. Ren, W. M. Liu, Y. L. Wang, J. C. Wang, Q. Tu, J. Xu, R. Liu, S. F. Shen and J. Wang, *Anal. Chem.*, 2013, **85**, 235-244.